

Matter-wave solitons in the counterflow of two immiscible superfluids

F. Tsitoura,¹ V. Achilleos,¹ B. A. Malomed,² D. Yan,³ P. G. Kevrekidis,³ and D. J. Frantzeskakis¹

¹*Department of Physics, University of Athens, Panepistimiopolis, Zografos, Athens 15784, Greece*

²*Department of Physical Electronics, School of Electrical Engineering,*

Faculty of Engineering, Tel Aviv University, Tel Aviv 69978, Israel

³*Department of Mathematics and Statistics, University of Massachusetts, Amherst MA 01003-4515, USA*

We study formation of solitons induced by counterflows of immiscible superfluids. Our setting is based on a quasi-one-dimensional binary Bose-Einstein condensate (BEC), composed of two immiscible components with large and small numbers of atoms in them. Assuming that the “small” component moves with constant velocity, either by itself, or being dragged by a moving trap, and intrudes into the “large” counterpart, the following results are obtained. Depending on the velocity, and on whether the small component moves in the absence or in the presence of the trap, two-component dark-bright solitons, scalar dark solitons, or multiple dark solitons may emerge, the latter outcome taking place due to breakdown of the superfluidity. We present two sets of analytical results to describe this phenomenology. In an intermediate velocity regime, where dark-bright solitons form, a reduction of the two-component Gross-Pitaevskii system to an integrable Mel’nikov system is developed, demonstrating that solitary waves of the former are very accurately described by analytically available solitons of the latter. In the high-velocity regime, where the breakdown of the superfluidity induces the formation of dark solitons and multi-soliton trains, an effective single-component description, in which a strongly localized wave packet of the “small” component acts as an effective potential for the “large” one, allows us to estimate the critical velocity beyond which the coherent structures emerge in good agreement with the numerical results.

PACS numbers: 03.75.Mn, 03.75.Lm, 05.45.Yv, 03.75.Kk

I. INTRODUCTION

Matter-wave solitons is a theme that has attracted much attention in studies of atomic Bose-Einstein condensates (BECs) [1, 2] and, more generally, in studies of superfluids [3] – see, e.g., recent reviews [4–6]. In atomic BECs, matter-wave solitons have been realized by means of various methods, including phase-imprinting [7], density engineering [8], quantum-state engineering [9], transport in optical lattices [10], transport past single defects [11] or through disordered potentials [12], and nonlinear interference between individual condensates [13]. Furthermore, matter-wave solitons have also been observed in multi-component BECs consisting of two different spin states of the same atom species. In particular, atomic dark-bright solitons have been realized in binary rubidium condensates by means of the quantum-state engineering technique [9], or the counterflow between two miscible components [14, 15]; employing the latter technique, generation of dark-dark solitons was reported too [16, 17]. Importantly, solitons have been argued to emerge spontaneously upon crossing the BEC phase transition, via the Kibble-Zurek mechanism [18]. This can be thought of as a quasi-one-dimensional analog of the pioneering experiments on the same mechanism in higher-dimensional BECs performed in [19].

As mentioned above, the counterflow of two miscible, quasi-one-dimensional (1D) BEC superfluids, is one of the techniques that were recently used for the generation of matter-wave solitons. More generally, the counterflow dynamics of superfluids is an interesting subject due to its links with such fundamental phenomena as turbulence, pattern formation, and generation of topological defects, which occur in a vast variety of physical contexts ranging from superfluid helium to cosmological strings and inflation [20]. In the context of binary atomic BECs, a number of theoretical works

have been dealing with the counterflow of either miscible [21, 22] or immiscible [23, 24] binary superfluids. In the former case, quantum turbulence and vortex generation in higher-dimensional settings [21] and in spinor BECs with $F = 1$ [22] were studied; in the latter case, effects of quantum swapping, Rayleigh-Taylor instability [23], and parametric resonance of capillary waves were predicted [24]. Furthermore, more recently, the counterflow superfluid of polaron pairs in Bose-Fermi mixtures in optical lattices was analyzed [25].

In the present work, we propose and analyze a physically relevant setting based on the counterflow of two immiscible superfluids. This setting can be used for the generation of scalar or vector solitons (of the dark-bright type) in binary BECs, and also for studies of their superfluid properties. We consider a quasi-1D binary BEC mixture composed of two immiscible components, “small” and “large” ones, with ratios of axial sizes and number of atoms in them $\sim 1 : 100$. We then assume that the “small” component moves with constant velocity v through the “large” one, by itself or being dragged by a moving trapping potential.

Systematic simulations of this setting produce the following phenomenology. For sufficiently small dragging velocities, $v < 0.61\tilde{c}_s$, with $c_s \equiv \sqrt{2}\tilde{c}_s$ being the speed of sound of the large component, and if the trap of the small component is switched off, the small component cannot remain localized, hence no well-defined patterns are formed. For intermediate velocities, $0.61\tilde{c}_s < v < 0.95\tilde{c}_s$, a robust two-component dark-bright soliton is formed. It is composed of a bright (dark) soliton in the small (large) component and can be very well approximated analytically. In particular, we use a multiscale asymptotic expansion method to reduce the underlying system of the Gross-Pitaevskii equations (GPEs) to a completely integrable Mel’nikov system [26], thus very accurately mapping the dark-bright solitary wave, which spontaneously emerges

in the GPE system, into an exact soliton of the Mel'nikov system. On the other hand, for $0.58\tilde{c}_s < v < 0.87\tilde{c}_s$ but in the presence of its trap dragging the small component, the ‘‘Mel'nikov's’’ dark-bright soliton still emerges but is unstable and eventually decays. For larger trap velocities, $v > 0.95\tilde{c}_s$, and if the trap is absent, a scalar dark soliton is created in the large component. Furthermore, for $v > 0.87\tilde{c}_s$ and in the presence of the trap, the small component is deformed into a sharply localized object, with a width on the order of the healing length, which propagates with a velocity larger than the critical velocity for the breakdown of the superfluidity in the large component. The breakdown leads to the emergence of multiple dark solitons, similarly to the results reported in previous theoretical [27, 28] and experimental [11] works (cf. also the quasi-two-dimensional analog of such an experiment producing vortex dipoles [29]).

The rest of the paper is structured as follows. The model is formulated in Section II. Then, in Section III, we systematically analyze, by means of analytical approximations and direct simulations, two different scenarios of the evolution of the small component, in the absence or in the presence of its trap. Finally, in Section IV we summarize our findings and discuss possibilities for the extension of the analysis.

II. THE MODEL AND SETUP

We consider the binary BEC composed of two hyperfine states of ^{87}Rb , that are described by macroscopic wave functions $\Psi_j(\mathbf{r}, t)$ ($j = 1, 2$). The dynamics can then be described by the following system of coupled GPEs [1, 2]:

$$i\hbar\partial_t\Psi_j = \left(-\frac{\hbar^2}{2m}\nabla^2 + V_j(\mathbf{r}) - \mu_j + \sum_{k=1}^2 g_{jk}|\Psi_k|^2 \right) \Psi_j, \quad (1)$$

where m is the atomic mass, μ_j are chemical potentials, $V_j(\mathbf{r})$ are trapping potentials, and $g_{jk} = 4\pi\hbar^2 a_{jk}/m$ are coupling constants defined by the s -wave scattering lengths, a_{jk} . Notice that, for states $|1, -1\rangle$ and $|2, 1\rangle$, which were used in the experiment of Ref. [30], or states $|1, -1\rangle$ and $|2, -2\rangle$ used in Refs. [14, 15], all the scattering lengths take approximately equal (positive) values. Below we assume $a_{11} = a_{22} \neq a_{12}$, hence the sign of parameter $\Delta \equiv (a_{11}a_{22} - a_{12}^2)/a_{11}^2$, which determines whether the two components are miscible ($\Delta > 0$) or immiscible ($\Delta < 0$) [31], depends only on ratio $\beta \equiv a_{12}/a_{11}$: if $\beta > 1$ ($\beta < 1$), then the two superfluids are immiscible (miscible).

We consider the case when both components are confined in strongly anisotropic (quasi-1D) traps, which have the form of rectangular boxes of lengths $L_{x_j} \gg L_{y_j} = L_{z_j} \equiv L_{\perp}$, with the transverse-confinement lengths L_{\perp_j} being on the order of the healing lengths ξ_j . For such a highly anisotropic trap, it is relevant to factorize the wave functions into longitudinal and transverse components, namely $\{u(x, t), v(x, t)\}$ and $\Phi_j(y, z)$ (see, e.g., Refs. [4–6]):

$$\Psi_1(\mathbf{r}, t) = \Phi_1(y, z)u(x, t)\exp(-iE_1t/\hbar), \quad (2)$$

$$\Psi_2(\mathbf{r}, t) = \Phi_2(y, z)v(x, t)\exp(-iE_2t/\hbar), \quad (3)$$

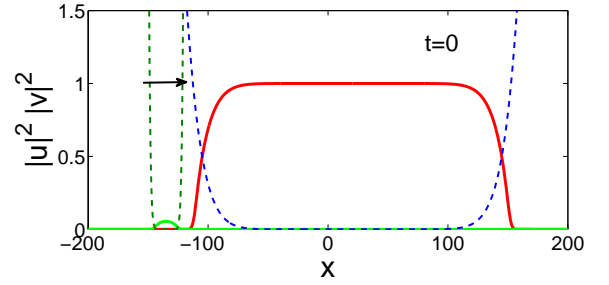


FIG. 1. (Color online) The density profiles (solid lines) of the two immiscible superfluids, confined by the box-shaped traps $V_1(x)$ and $V_2(x, t)$ (dashed lines) at $t = 0$. The red (green) line corresponds to the u - (v -) component. The arrow depicts the direction of motion of the v -component at $t > 0$.

where the transverse modal functions $\Phi_j(y, z)$ and energies E_j are determined by the auxiliary 2D problem for the quantum oscillator in the transverse box. Since the considered system is effectively one-dimensional, it is natural to assume that Φ_j remains in the ground state, i.e., $\Phi_j(y, z) = (\sqrt{2}/L_{\perp})\sin(\pi y/L_{\perp})\sin(\pi z/L_{\perp})$, for $j = 1, 2$. Using these expressions, we substitute expressions (2)–(3) into Eqs. (1) and perform averaging over the transverse coordinates, to derive a system of scaled equations for the longitudinal wave functions $u(x, t)$ and $v(x, t)$ (see also Ref. [32]):

$$iu_t = -u_{xx} + (|u|^2 + \beta|v|^2 - \mu_1)u + V_1(x)u, \quad (4)$$

$$iv_t = -v_{xx} + (\beta|u|^2 + |v|^2 - \mu_2)v + V_2(x)v, \quad (5)$$

where subscripts stand for partial derivatives. In these equations, longitudinal coordinate x , time t , densities $|u|^2$, $|v|^2$, and energy are measured, respectively, in units of the healing length $\xi_1 \equiv \hbar/\sqrt{2mn_1\tilde{g}_{11}}$, characteristic time $\sqrt{2}\xi_1/c_s$ (where $c_s \equiv \sqrt{\tilde{g}_{11}n_1/m}$ is the sound speed of the first component), density n_1 , and characteristic energy $\tilde{g}_{11}n_1$ of the first component. Finally, $\tilde{g}_{ij} = (9/4L_{\perp}^2)g_{ij}$ are the effective 1D interaction strengths.

It is now useful to adopt experimentally relevant values of the parameters. First, we fix the scattering length and the density of first component to $a_{11} = 5.77 \text{ nm}$ and $n_1 = 10^8 \text{ m}^{-3}$, which results in the healing length, $\xi_1 = 0.25 \mu\text{m}$; next, we fix $\beta = 1.1$, which corresponds to the immiscibility (we have checked that other values of $\beta > 1$ lead to qualitatively similar results). We will assume that the first component (u) is ‘‘much larger’’ than the other one (v), in the sense that the respective ratio of the numbers of atoms is $N_1/N_2 \approx 100$; accordingly, the chemical potentials are fixed to $\mu_1 = 1$ and $\mu_2 = 0.06$. As concerns the size of the traps, we assume that, in most cases, $L_{x_1} = 57.6 \mu\text{m}$, $L_{x_2} = 5 \mu\text{m}$, and $L_{\perp} = 0.8 \mu\text{m}$, which correspond, respectively, to $L_{x_1} = 244$, $L_{x_2} = 21$ and $L_{\perp} = 3$ in the dimensionless units; an exception concerns Fig. 5 (see below), where we use $L_{x_1} = 123 \mu\text{m}$ (or 490 in the dimensionless units) for the length of the u -component. We have checked that, as long as the ratios of the atom numbers, chemical potentials and trap lengths are such that $N_1/N_2 \sim \mu_1/\mu_2 \sim 100$ and $L_{x_1} : L_{x_2} : L_{\perp} \sim 100 : 10 : 1$, the results are qualitatively similar.

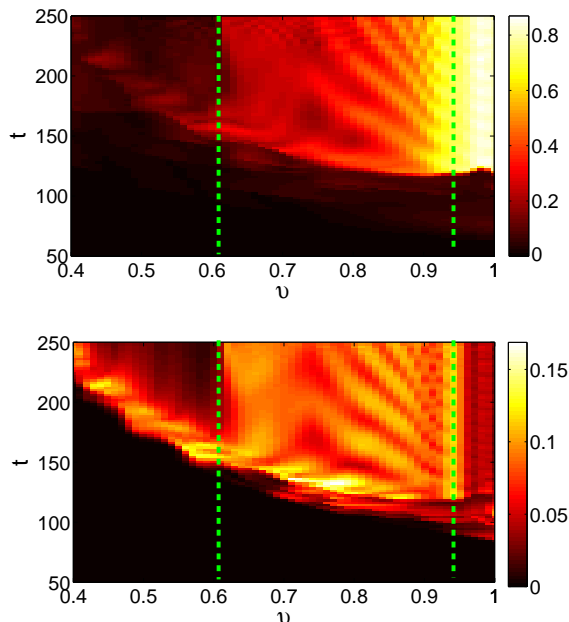


FIG. 2. (Color online) Contour plots showing the evolution of the largest density dip in the u -component (the top panel) and the peak density of the v -component (the bottom panel), with respect to the velocity of the motion of the trap. We identify three different regimes, separated by the vertical (green) dashed lines: a) $0 < v < 0.61$, where no localized excitations are formed, b) $0.61 < v < 0.95$, where traveling dark-bright solitons emerge, and c) $v > 0.95$, where deep dark solitons are formed in the u -component. In the latter case, the v -component is quickly dispersed.

In our simulations, we will approximate the box-like trapping potentials V_j by super-Gaussians:

$$V_j = V_0 \left[1 - \exp \left(- \left(\frac{x + x_j}{w_j} \right)^{12} \right) \right], \quad (6)$$

where V_0 is the (common) trap amplitude for both components, while x_j and w_j denote the positions and widths of the traps, respectively. We fix these parameters as $V_0 = 10$, $x_1 = -20$, $w_1 = 160$, and $w_2 = 20$; as concerns the position of the trap acting on the v -component, it is assumed to be initially (at $t = 0$) placed at $x_2(0) = 135$ and move at a constant velocity: $x_2 = 135 - vt$. Thus, the “small” v -component starts moving to the right, penetrating the “large” u -component; notice that v is measured in units of $\tilde{c}_s = c_s/\sqrt{2}$ (recall that c_s is the speed of sound of the u -component). As we show below, such an effective counterflow gives rise to the formation of nonlinear structures and solitons that we will investigate in detail in the following section. Furthermore, we note in passing that in the immiscible case considered here, the counterflow with speed v is modulationally stable, in accordance with the criterion of [14, 16]. This can also be intuitively understood on the basis of immiscibility of two independently modulationally stable components.

The initial configuration, obtained by means of an imaginary-time integration, is depicted in Fig. 1, where the

two components are initially separated. Then, at $t > 0$, the v -component is set into motion and moves through the u -component. The evolution of the system is monitored by numerically integrating Eqs. (4) and (5) in real time by means of the split-step Fourier method.

III. ANALYTICAL AND NUMERICAL RESULTS

We will consider two different cases: (A) when trap V_2 , acting on the small component, is switched off after it has penetrated the u -component (for the above-mentioned parameters, this occurs at $x = -40$ and $t \sim 100$); (B) the trap V_2 is not switched off, i.e., the v -component is permanently dragged by its trap.

A. Evolution of the small component in the absence of the trap.

In this case, our systematic simulations have revealed the existence of three different velocity regimes, characterized by the emergence (or the failure to emerge) of various localized nonlinear structures. These regimes were identified by calculating – at each time step – the maximum density dip in the u -component, as well as the peak density of the v -component, as shown in the top and bottom panel of Fig. 2, respectively.

In particular, for velocities $0 < v < 0.61$ [corresponding to the region on the left of the first dashed (green) line in Fig. 2], no clear solitary-wave structure is formed in the dynamics. There exist, however, numerous small-amplitude dips that are formed in the u -component, which propagate with speeds approximately equal to the speed of sound in that component. Generally, for such relatively small velocities, as long as the v -component penetrates the u -component, strong emission of radiation is observed. A typical example is shown in Fig. 3, for $v = 0.3$. In addition to the small-amplitude sound wavepackets propagating in the u component, there exists a slow structure (with a speed near close to that of the initially moving trap), which emerges with a larger dip in the u -component and a bright “bump” in the v component. Yet, this structure does not preserve its shape, but rather slowly disperses, contrary to what would be expected of a robust solitary wave.

On the other hand, in the intermediate velocity regime, $0.61 < v < 0.95$ [see the region between dashed (green) lines in Fig. 2], the v -component forms a relatively large peak, which is practically robust and does not decay in time. Additionally, a dip of a constant density is formed in the large (u) component, which propagates with the same velocity as the peak in the the v -component, i.e., the two components build a traveling coherent structure. An example, shown in the top panel of Fig. 4 for $v = 0.7$, reveals this in more detail: after a relatively short transient period ($t \simeq 100$) needed for the v -component to reach the flat segment of the u -component, a small-amplitude dark-bright soliton is formed. Notice that the strong emission of sound waves –which is observed chiefly in the u -component– is solely due to the penetration process (as in the case of Fig. 3): the sound waves get detached from the

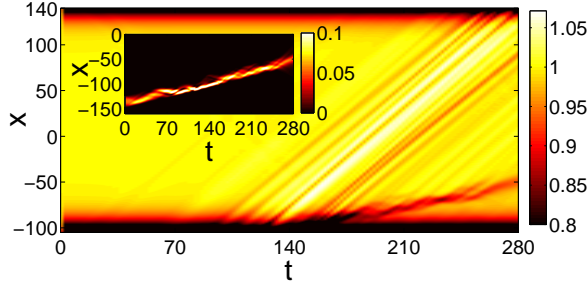


FIG. 3. (Color online) Contour plots showing the evolution of the density of the u -component (the inset shows the evolution of the v -component) for trap's velocity $v = 0.3$. It is observed, aside from the emission of sound waves in the u -component, that a structure resembling a dark-bright solitary wave is formed. However, it slowly disperses in the course of the evolution.

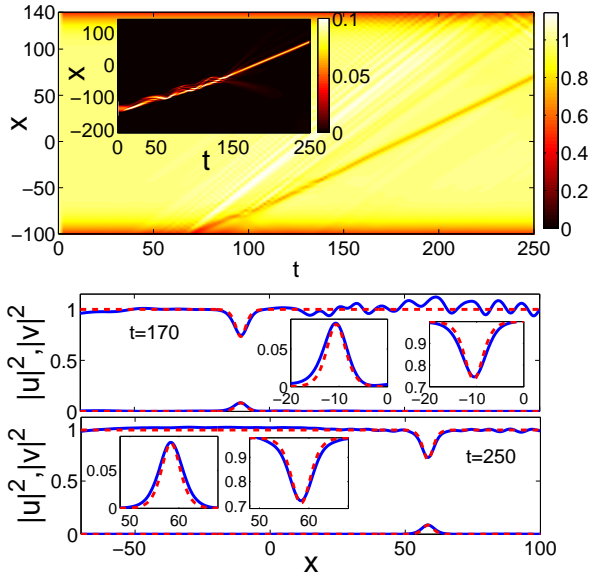


FIG. 4. (Color online) The top panel shows the evolution of the density the u -component (inset shows the evolution of the v -component) for trap's velocity $v = 0.7$. It is observed that a Mel'nikov's soliton, moving with a velocity $v_{\text{sol}} = 0.96$, is formed. The middle and bottom panels show snapshots of the densities of the dark soliton in the u -component, and the bright soliton in the v -component, for $t = 170$ and $t = 250$, respectively. Solid (blue) and dashed (red) lines represent the numerical and analytical results, the agreement between which is excellent.

subsonic dark-bright soliton shortly after its generation, and the soliton propagates undistorted thereafter over the spatial region occupied by the u -component.

To get a deeper insight into the solitary-wave formation, we apply an asymptotic multiscale expansion method to Eqs. (4) and (5). In particular, considering only the flat region of the u -component (where the soliton formation is observed), we neglect the trapping potentials $V_{1,2}$ in Eqs. (4)-(5) (recall that V_2 is switched off in the region where $V_1 = 0$ and the u -component is practically flat), and assume that chemical potential μ_2 is small. We thus introduce a formal small param-

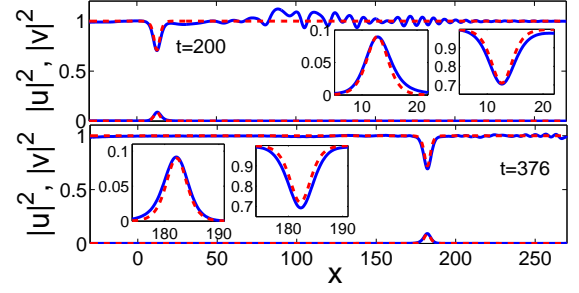


FIG. 5. (Color online) The same as in the middle and bottom panels of Fig. 4, but for a larger size of trap V_1 , namely $L_{x_1} = 123 \mu\text{m}$ (or $L_{x_1} = 490$ in dimensionless units). In this case, as shown in the snapshots at $t = 200$ (the top panel) and $t = 376$ (the bottom panel), the evolution time of the Mel'nikov soliton is significantly longer.

eter ε which measures the smallness of the chemical potential of the v -component, and substitute $\mu_2 \rightarrow \varepsilon\mu_2$ in Eqs. (4)-(5). Our main goal is to reduce the original system of Eqs. (4)-(5) to a simpler one, namely the completely integrable Mel'nikov system [26], which will provide an analytical description of the vector soliton observed in Fig. 4.

The analysis starts by introducing the ansatz,

$$u = \sqrt{\rho} \exp(i\varphi), \quad v = q \exp(i\theta), \quad (7)$$

$$\theta = \sqrt{\frac{\mu_1}{2}} x - \left[\mu_1 \left(\frac{1}{2} + \beta \right) + \varepsilon\Omega \right] t, \quad (8)$$

where real functions $\rho(x, t)$ and $\varphi(x, t)$ denote the amplitude and phase of the u -component, while $q(x, t)$ and $\theta(x, t)$ represent a (complex) amplitude and phase of the v -component. As we will see below, Ω is related to the amplitude of the dark soliton in the u -component.

Substituting Eqs. (7)-(8) into Eqs. (4)-(5), we obtain the following system of equations for fields ρ , φ and q :

$$\varphi_t + \rho + \beta|q|^2 - \mu_1 + \varphi_x^2 - \rho^{-1/2}(\rho^{1/2})_{xx} = 0, \quad (9)$$

$$\frac{1}{2}\rho_t + (\rho\varphi_x)_x = 0, \quad (10)$$

$$i \left(q_t + \sqrt{2\mu_1} q_x \right) + q_{xx} - [|q|^2 - \beta(\mu_1 - \rho)]q + \varepsilon(\mu_2 + \Omega)q = 0. \quad (11)$$

Next, we define the slow variables:

$$T = \varepsilon^{3/2}t, \quad X = \varepsilon^{1/2}(x - c_s t), \quad (12)$$

where c_s is an unknown velocity, to be determined in a self-consistent manner. Additionally, we express unknown fields ρ , φ and q as asymptotic series in ε :

$$\rho = \mu_1 + \varepsilon\rho_1(X, T) + \varepsilon^2\rho_2(X, T) + \dots, \quad (13)$$

$$\varphi = \varepsilon^{1/2}\varphi_1(X, T) + \varepsilon^{3/2}\varphi_2(X, T) + \dots, \quad (14)$$

$$q = \varepsilon q_1(X, T) + \varepsilon^2 q_2(X, T) + \dots \quad (15)$$

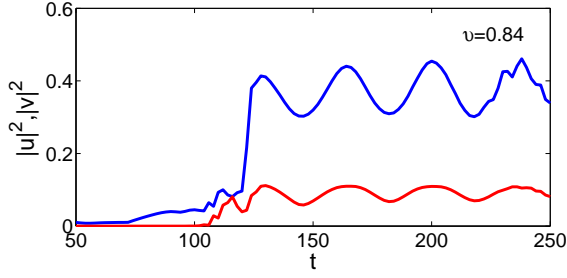


FIG. 6. (Color online) The evolution of the largest density dip in the u -component [the upper (blue) line] and peak density of the v -component [the lower (red) line], for the trap's velocity $v = 0.84$.

Substituting expansions (13)-(14) into Eqs. (9)-(10), at the leading-order of approximation, i.e., at orders $\mathcal{O}(\varepsilon)$ and $\mathcal{O}(\varepsilon^{3/2})$, compatibility conditions of the resulting equations lead to the following results. First, we determine the unknown velocity $c_s \equiv \sqrt{2\hat{c}_s}$, which turns out to be the speed of sound of the u -component:

$$c_s = \pm \sqrt{2\mu_1}, \quad (16)$$

and derive an equation connecting unknown phase φ_1 with amplitude ρ_1 :

$$\varphi_X = c_s^{-1} \rho_1. \quad (17)$$

Proceeding to the next orders, i.e., $\mathcal{O}(\varepsilon^2)$ and $\mathcal{O}(\varepsilon^{5/2})$, the compatibility condition for the respective equations ensuing from Eqs. (9)-(10) yields the following nonlinear equation:

$$2\rho_{1T} + \frac{6}{c_s} \rho_1 \rho_{1X} - \frac{c_s}{2} \rho_{1XXX} + c_s \beta (|q_1|^2)_X = 0. \quad (18)$$

At the order $\mathcal{O}(\varepsilon^2)$, Eq. (11) is reduced to the following equation:

$$q_{1XX} - \beta \rho_1 q_1 + (\mu_2 + \Omega) q_1 = 0. \quad (19)$$

The system of Eqs. (18)-(19) represents the Korteweg-de Vries (KdV) equation with a self-consistent source, which is determined by a stationary Schrödinger equation, is the Mel'nikov system [26], which is *completely integrable* and possesses exact soliton solutions of the form:

$$\rho_1 = -\frac{2\delta}{\beta} \text{sech}^2 \eta, \quad (20)$$

$$q_1 = b \exp(-i\omega_0 T) \text{sech} \eta, \quad (21)$$

where $\eta = \sqrt{\delta}(X + VT)$, with V being the soliton velocity, and ω_0 is an arbitrary constant. Further, parameters $\delta \equiv \mu_2 + \Omega$ and b (which set the amplitudes of ρ_1 and q_1 , respectively), are related to the soliton velocity via the equation:

$$b^2 = \frac{4\delta}{\beta^2 c_s} (V - \delta c_s). \quad (22)$$

Obviously, the velocity of the Mel'nikov's soliton is bounded from below, *viz.*, $V \geq V_{\text{cr}} \equiv \delta c_s$, which follows from the condition that b^2 is real.

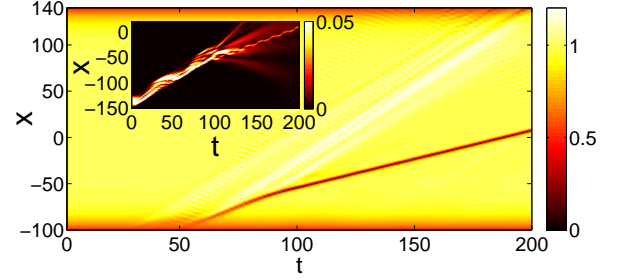


FIG. 7. (Color online) The same as in the top panel of Fig. 4, but for the trap's velocity $v = 1$. In this case, although the v -component is quickly dispersed (and dark-bright solitons cannot be formed), it creates a robust dark soliton in the u -component.

Using the above results, we can now write down an approximate [valid up to order $\mathcal{O}(\varepsilon)$] soliton solution of Eqs. (4)-(5). This solution is a vectorial soliton, composed of a dark soliton in the u -component, coupled to a bright soliton in the v -component. In terms of the original variables x and t , it is expressed as follows:

$$u(x, t) \approx \left(\mu_1 - \frac{\varepsilon \delta}{\beta} \text{sech}^2 \eta \right) \exp \left(i \sqrt{\varepsilon \delta} c_s^{-1} \tanh \eta \right), \quad (23)$$

$$v(x, t) \approx \varepsilon b \text{sech} \eta \exp(i\theta), \quad (24)$$

where $\eta \equiv \sqrt{\varepsilon \delta}(x - v_{\text{sol}} t)$, with $v_{\text{sol}} \equiv c_s - \varepsilon V$ being the velocity of the soliton. Note that this solution is characterized by two independent parameters, which set the dark- and bright-soliton's amplitudes, $\varepsilon \delta$ and εb . These parameters determine the soliton's velocity too, via Eq. (22).

This analytical result is compared to results of the numerical simulations in the middle and bottom panels of Fig. 4: upon numerically determining the soliton's amplitudes, and finding its velocity by means of Eq. (22), we can analytically determine the soliton density profiles [dashed (red) lines] and compare them to the ones found by the direct numerical integration of Eqs. (4)-(5) [solid (blue) lines]. In this way, we find that the dark and bright soliton's amplitudes are $\varepsilon \delta = 0.27$ and $(\varepsilon b)^2 = 0.08$, respectively, and the numerically found soliton velocity is 0.88. The latter value is in excellent agreement with the analytical prediction, $v_{\text{sol}} = 0.89$. This is also directly observed in Fig. 4, where the analytical predictions [dashed (red) lines] are compared to results of the simulations [solid (blue) lines], see the snapshots corresponding to $t = 170$ (middle panel) and $t = 250$ (bottom panel). A similar excellent agreement is observed in Fig. 5, but for a longer propagation time (for trap V_1 of a larger size, $L_{x_1} = 123 \mu\text{m}$, or $L_{x_1} = 490$ in the dimensionless notation). We note in passing that we have also checked that the Mel'nikov dark-bright soliton remains robust after its reflection from the trap boundaries and its interaction with the sound waves.

Coming back to Fig. 2, it is observed that, close to the right edge of the intermediate velocity regime, *viz.*, at $0.8 \lesssim v < 0.95$, the solitons undergo a transient behavior: their peak densities perform breathing oscillations, as shown in Fig. 6 for $v = 0.84$. Clearly, this type of the behavior cannot be captured by the Mel'nikov model (which does not give rise to

breathing modes). After this transient region, in the regime of a large trap velocity, $v > 0.95$, the v -component does not stay localized and is quickly dispersed; this can also be observed in Fig. 2. Thus, in this case, the dark-bright soliton of the Mel'nikov type is not formed. However, shortly after penetrating the u -component, the v -component creates a dark soliton there, which propagates robustly all over the spatial region occupied by the u -component, cf. Fig. 7 for $v = 1$.

To summarize, in this case of the v -component trap was switched off, we have identified three basic regimes. For small initial trap's speeds, the u and v components are too slow for combining into one of the higher-speed Mel'nikov-type dark-bright solitons. For the trap's speed which is too large, the intrusion of the v component into u produces a single dark soliton, but subsequently the v component disperses fast, without creation of other coherent structures. In the intermediate regime, the two components can "lock" into a dark-bright solitary wave, which can be mapped into the solitons of the Mel'nikov model.

B. Evolution of the small component in the presence of the trap.

We now consider the case when trap V_2 is not switched-off and, thus, the v -component evolves in the presence of its trap. The pertinent contour plots depicting the largest dip in the u -component and the peak density of the v -component are shown in the top and bottom panels of Fig. 8, respectively. Similarly to the case without the trap, three different regimes can be identified. In particular, for low trap velocities $v < 0.58$, the dynamics of the two components is similar to that observed in Fig. 3. Again, in this case, long-lived localized structures are not formed in either component, and strong emission of radiation is observed.

For the trap velocity in the intermediate region of $0.58 < v < 0.87$ [see the region in between the two dashed (green) lines in Fig. 8], we find that dark-bright solitons of the Mel'nikov type are again formed (as in the previous case where the trap v_2 was switched off), but they eventually decay. A typical example of this behavior is shown in Fig. 9, for $v = 0.8$. As is observed in the inset of the figure, after the v -component has intruded into the u -field, it splits into fragments, following its in-trap dynamics. The largest one among these fragments couples to a dark soliton in the u -component, and the resulting structure can be categorized as a Mel'nikov soliton: for the parameters used in Fig. 9, the numerically found average dark and bright soliton's amplitudes are $\varepsilon\delta \approx 0.26$ and $(\varepsilon b)^2 \approx 0.08$, which correspond to the soliton's velocity [found via Eq. (22)] $v_{\text{sol}} \approx 1.1$. This is in good agreement with the numerically found mean soliton's velocity, which is ≈ 1 , a fact that indicates that this structure is indeed proximal to a Mel'nikov soliton. However, in the case of Fig. 9, the v -component travels with speed $v = 0.8$, while the soliton propagates with a larger velocity. Therefore, the confined bright-soliton component inevitably collides with – and is reflected by – the trap boundaries. This results in complex motion of the dark-bright soliton, which cannot be sustained

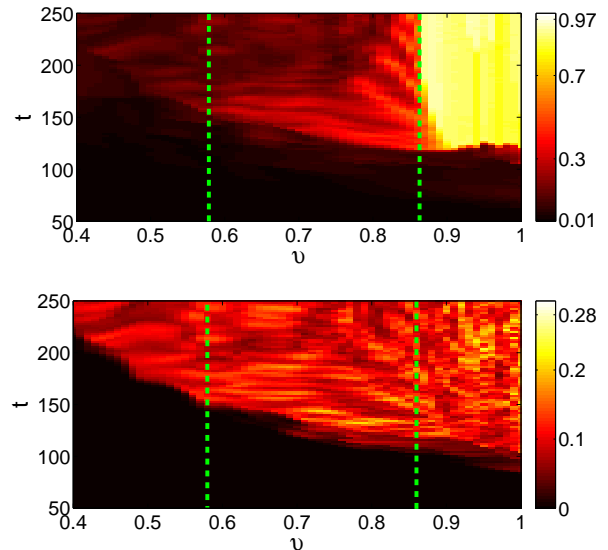


FIG. 8. (Color online) The same as in Fig. 2, but in the case when the v -component is subject to the action of the trap. In this case too, three different regimes can be identified: a) $0 < v < 0.58$ with no localized excitations, b) $0.58 < v < 0.87$, where unstable dark-bright solitons are observed, and c) $v > 0.87$, in which case we observe the nucleation of multiple dark solitons in the u -component.

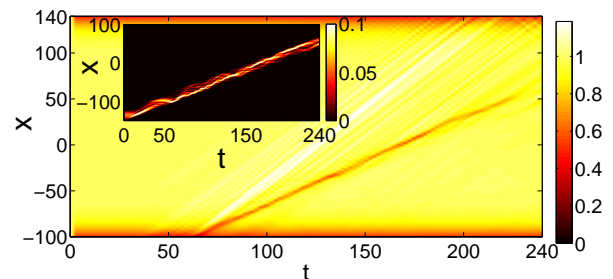


FIG. 9. (Color online) The same as in the top panel of Fig. 4, but for the trap's velocity $v = 0.8$. In this case, a dark-bright soliton of the Mel'nikov type is formed, but it decays due to the fact that the soliton's velocity is larger than the speed of the trap (see text).

for long times and eventually decays (at $t \sim 200$). In fact, it is the trap itself in this case which is detrimental to the existence of the Mel'nikov soliton. While the latter has its intrinsic velocity upon the formation, the trap bears its own distinct velocity, and, barring a non-generic scenario when these two velocities coincide, we cannot expect the solitary wave to persist, due to the unavoidable collision with either the "front" or the "back" of the trap. This is the key distinguishing feature between the intermediate speed cases in the presence and absence of the trap.

When the trap's velocity exceeds the value $v = 0.87$, we observe a constant robust large dip, in the u -component, while the v -component features a peak, oscillating around a relatively large value. As we show below, this is a critical velocity above which multiple dark solitons are generated in the u -component, indicating breakdown of the superfluidity. As

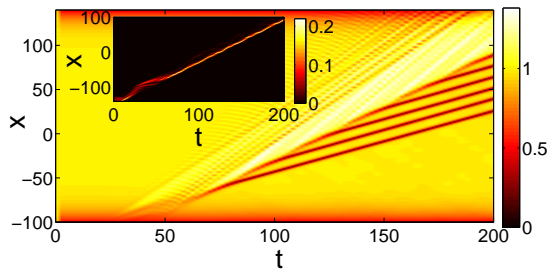


FIG. 10. (Color online) The top panel is the same as in Fig. 4, but for the trap’s velocity $v = 1.2$. In this case, the superfluidity of the u -component breaks down, and multiple dark solitons are formed.

shown in the top panel of Fig. 8, a persistent, almost zero-density region arises in the u -component. In this case, the nucleation of multiple dark solitons in the u -component occurs. A typical example is shown in the top panel of Fig. 10 (for $v = 1.2$): shortly after the v -component has intruded into the flat part of the u -component, dark solitons are repeatedly emitted. This behavior can be understood as the breakdown of the superfluidity in the u -component, caused by the supersonic motion of the v -component: in fact, as shown in the bottom panel of Fig. 10, at early stages of the evolution, the v -component actually becomes a sharply localized “obstacle”, which moves with a velocity exceeding the critical one (which is, roughly, the speed of sound c_s of the u -component). Accordingly, the dynamics follows the scenario revealed in previous theoretical [27, 28] and experimental [11] works concerning the breakdown of the superfluidity in quasi-1D BECs. In all these works, continuous emission of dark solitons was reported. The mechanism of the breakdown was elucidated in the pioneering work of Hakim [27]. In particular, up to the critical point, the moving defect (in our case, the effective one, represented by the v -component) can sustain a pair of localized states co-traveling with it (a saddle and a center). Past the critical point, a saddle-center bifurcation arises, and such states can no longer be sustained. To alleviate the local super-criticality (in terms of the speed), the defect nucleates a (sub-sonic) dark solitary wave. Yet, once the wave has traveled sufficiently far downstream, it no longer renders the vicinity of the defect sub-critical, and a new dark soliton is emitted. The repetition of this process leads to the emergence of a dark-soliton train.

It is relevant to quantitatively justify the above arguments, upon estimating the critical velocity needed for the breakdown of the superfluidity. This can be done as follows. First, we observe, in the example depicted in Fig. 11 for $v = 0.8$, that the v -component has initially (at $t = 0$) the form of an extended wave packet (shaped by trap acting on it); however, after intruding into the u -field, it splits into fragments. The largest among these fragments has the peak density approximately four times as large as the initial one, and becomes sharply localized, with the half-width at half-maximum of the order of healing length ξ (which is equal to 1 in our dimensionless notation). Based on this observation, it is possible to consider the v -component as a delta-like obstacle of some effective strength v_* . To calculate it, we fit the v -component

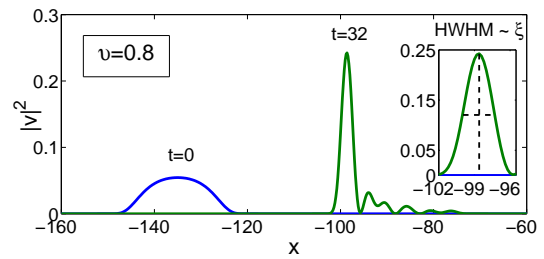


FIG. 11. (Color online) The plot shows the density of the v -component for the trap’s velocity $v = 0.8$, in two instants: at $t = 0$ (the blue line) and at $t = 32$ (the green line), when it attains the maximum peak density. The inset shows the density profile of the larger part of the v -component at $t = 32$; its half-width at half-maximum (HWHM) equals to 1.3, being on the order of the healing length, ξ .

by a normalized Gaussian function with an equal amplitude at $t \sim 32$ (when the v -component attains its maximum peak density). Then, we use the approximate expression for the critical velocity of Ref. [27], which reads:

$$v_* = 4(1 - v_{cr}^2/2) \frac{[\sqrt{1 + 4v_{cr}^2} - (1 + v_{cr}^2)]^{1/2}}{2v_{cr}^2 - 1 + \sqrt{1 + 4v_{cr}^2}}. \quad (25)$$

In Fig. 12, we show the dependence of the critical velocity v_{cr} , calculated as explained above, on the trap’s velocity v . By applying a straight-line fit to the values of v_{cr} , we find that $v_{cr} \approx 0.048v + 0.832$. Thus, there is a very weak dependence of the effective strength of amplitude of the steep moving obstacle, represented by the v -component, on the initial trap’s speed. By comparing this fit with the diagonal in the (positive quarter-) plane of v_{cr} vs. v , we can conclude what initial speeds of the trap turn out to be supercritical. In particular, it is clear from Fig. 12 that, for $v > 0.874$, the trap exceeds the critical velocity v_{cr} , hence the superfluidity is expected to break down. Note that the numerically obtained velocity, beyond which the superfluidity breaks down indeed and dark solitons are emitted was found to be $v = 0.87$ [see the rightmost dashed (green) lines in Fig. 8], which is in excellent agreement with the theoretical approximation based on Eq. (25).

In summary, three regimes are also identified in the case when the v -component is subject to the action of the potential, although their dynamics is different from the case when the trap was absent, except for the low-speed case. In the intermediate-speed regime, solitary waves of the Mel’nikov type form but are unstable due to the velocity mismatch with the moving trap. In the large-speed regime, the superfluidity was shown to break down at the critical point very close to the related analytical prediction, which leads, as in the case of Ref. [27], to the emission of a train of dark solitons, due to the effective potential exerted by the second (v) component on the first (u) one.

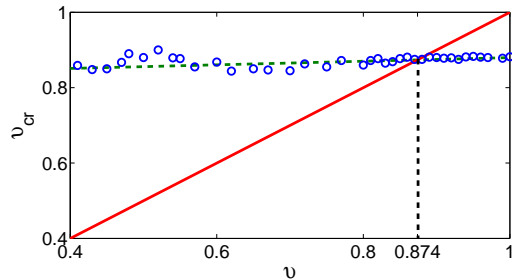


FIG. 12. (Color online) The critical velocity, v_{cr} , versus the trap's velocity, v . First we calculate the value of v_{cr} [depicted by (blue) circles] for different trap's velocities, and then apply the straight-line fit [the dashed (green) line]. Breakup of the superfluidity is expected when the trap's velocity becomes larger than the critical velocity, i.e. at $v \approx 0.874$, as indicated by the vertical dashed (black) line.

IV. CONCLUSIONS.

In this work, we have studied the dynamics of two quasi-1D counter-propagating immiscible superfluids. Our setup is based on the BEC mixture composed by two different spin states of the same atomic species, with the number of atoms in one of the two components being much smaller than in the other. In our simulations of the coupled GPEs, we have assumed that the “large” component is at rest while the “small” component starts intruding into the larger one, moving at a constant velocity v .

We have considered two different situations, namely, with the small component propagating either in the absence or in the presence of the trap. For sufficiently small trap's velocities v , we have found that no localized structures emerge.

On the other hand, for intermediate velocities in the interval of $0.61\tilde{c}_s < v < 0.95\tilde{c}_s$, if the trap acting on the small component is switched off, we have found that a robust dark-bright soliton is formed. This structure is composed of a bright (dark) soliton in the small (large) component, and can be very well approximated analytically by means of the multiscale asymptotic expansion method, which reduces the original GPE system to the completely integrable Mel'nikov system. This system has exact soliton solutions that can be used to construct the approximate dark-bright soliton solutions of the GPE system. We have also found that, if the small component is subject to the action of the trapping potential, then the Mel'nikov-type dark-bright soliton forms in a similar velocity regime, $0.58\tilde{c}_s < v < 0.87\tilde{c}_s$, but it cannot be sustained due

to the mismatch between its own velocity and the speed of the moving trap.

If the small component propagates in the absence of the trap, then, for large initial trap velocities, $v > 0.95\tilde{c}_s$, it disperses and no dark-bright soliton is formed; nevertheless, a dark soliton is always created in the large component. On the other hand, if the small component propagates in the presence of its trap, which moves with speed $v > 0.87\tilde{c}_s$, we have found that it gets deformed into a sharply localized object of the width on the order of the healing length, which propagates with a velocity larger than the critical velocity of the large component. Approximating the small component by an effective delta-like obstacle acting on the large component, we have found that, in the case of such large trap velocities, the dynamics of the system follows the scenario known for the quasi-1D superfluid flow past an obstacle. In this way, the superfluidity of the large component breaks down, and nucleation of a train of dark solitons occurs.

Our results suggest that such counterflow settings may be quite relevant to the observation of fundamental phenomena, such as the formation of solitons and/or the identifying the critical velocity in superfluid flows. It would be interesting to extend the considerations to higher-dimensional settings and, also, to larger number of components, as, e.g., in the case of $F = 1$ or $F = 2$ spinor BECs [33]. In that case, vortex-bright solitary waves [34] and their dipole-more generalizations [35] are expected to arise, as well as their spinor counterparts. The generalizations with a larger number of components and in higher dimensions is likely to produce novel waveforms. Another relevant extension concerns the role of g_{12} (the cross-component interaction strength) and the approach to the miscibility-immiscibility threshold. In that context, exploring the conditions under which additional waveforms (such as dark-dark solitons of [16, 17] and their multi-dimensional counterparts) can arise would also be a theme of interest. These topics are currently under investigation and will be reported elsewhere.

Acknowledgments. Constructive discussions with P. Engels are kindly acknowledged. V.A. appreciates financial support from A. G. Leventis Foundation. The work of D.J.F. was partially supported by the Special Account for Research Grants of the University of Athens. P.G.K. gratefully acknowledges support from the Alexander von Humboldt Foundation and from the NSF under grant DMS-0806762. The work of P.G.K. and B.A.M. was supported, in a part, by the Binational (US-Israel) Science Foundation under grant No. 2010239.

-
- [1] C. J. Pethick and H. Smith, *Bose-Einstein condensation in dilute gases* (Cambridge University Press, Cambridge, 2002).
 - [2] L. P. Pitaevskii and S. Stringari, *Bose-Einstein Condensation* (Oxford University Press, Oxford, 2003).
 - [3] G. E. Volovik, *The Universe in a Helium Droplet* (Oxford University Press, Oxford, 2003).
 - [4] P. G. Kevrekidis, D. J. Frantzeskakis, and R. Carretero-

González, *Emergent Nonlinear Phenomena in Bose-Einstein Condensates: Theory and Experiment* (Springer-Verlag, Heidelberg, 2008).

- [5] R. Carretero-González, D. J. Frantzeskakis, and P. G. Kevrekidis, *Nonlinearity* **21**, R139 (2008).
- [6] D. J. Frantzeskakis, *J. Phys. A: Math. Theor.* **43**, 213001 (2010).
- [7] S. Burger, K. Bongs, S. Dettmer, W. Ertmer, K. Sengstock,

- A. Sanpera, G. V. Shlyapnikov and M. Lewenstein, Phys. Rev. Lett. **83** 5198 (1999); J. Denschlag, J. E. Simsarian, D. L. Feder, C. W. Clark, L. A. Collins, J. Cubizolles, L. Deng, E. W. Hagley, K. Helmerson, W. P. Reinhardt, S. L. Rolston, B. I. Schneider, and W. D. Phillips, Science **287**, 97 (2000); S. Stellmer, C. Becker, P. Soltan-Panahi, E.-M. Richter, S. Dörscher, M. Baumert, J. Kronjäger, K. Bongs, and K. Sengstock, Phys. Rev. Lett. **101**, 120406 (2008).
- [8] Z. Dutton, M. Budde, C. Slowe, and L. V. Hau, Science **293**, 663 (2001).
- [9] C. Becker, S. Stellmer, P. Soltan-Panahi, S. Dörscher, M. Baumert, E.-M. Richter, J. Kronjäger, K. Bongs, and K. Sengstock, Nature Phys. **4**, 496 (2008).
- [10] R. G. Scott, A. M. Martin, T. M. Fromhold, S. Bujkiewicz, F. W. Sheard, and M. Leadbeater, Phys. Rev. Lett. **90** 110404 (2003); R. G. Scott, A. M. Martin, S. Bujkiewicz, T. M. Fromhold, N. Malossi, O. Morsch, M. Cristiani, and E. Arimondo, Phys. Rev. A **69**, 033605 (2004).
- [11] P. Engels and C. Atherton, Phys. Rev. Lett. **99**, 160405 (2007).
- [12] M. Albert, T. Paul, N. Pavloff, and P. Leboeuf, Phys. Rev. Lett. **100**, 250405 (2008); D. Dries, S. E. Pollack, J. M. Hitchcock, and R. G. Hulet, Phys. Rev. A **82**, 033603 (2010).
- [13] A. Weller, J. P. Ronzheimer, C. Gross, J. Esteve, M. K. Oberthaler, D. J. Frantzeskakis, G. Theocharis, and P. G. Kevrekidis, Phys. Rev. Lett. **101**, 130401 (2008); I. Shomroni, E. Lahoud, S. Levy and J. Steinhauer, Nat. Phys. **5** 193 (2009); G. Theocharis, A. Weller, J. P. Ronzheimer, C. Gross, M. K. Oberthaler, P. G. Kevrekidis, and D. J. Frantzeskakis, Phys. Rev. A **81**, 063604 (2010).
- [14] C. Hamner, J. J. Chang, P. Engels, M. A. Hoefer, Phys. Rev. Lett. **106**, 065302 (2011).
- [15] S. Middelkamp, J. J. Chang, C. Hamner, R. Carretero-González, P. G. Kevrekidis, V. Achilleos, D. J. Frantzeskakis, P. Schmelcher, and P. Engels, Phys. Lett. A **375**, 642 (2011); D. Yan, J. J. Chang, C. Hamner, P. G. Kevrekidis, P. Engels, V. Achilleos, D. J. Frantzeskakis, R. Carretero-González, and P. Schmelcher, Phys. Rev. A **84**, 053630 (2011).
- [16] M. A. Hoefer, J. J. Chang, C. Hamner, and P. Engels, Phys. Rev. A **84**, 041605(R) (2011).
- [17] D. Yan, J. J. Chang, C. Hamner, M. A. Hoefer, P. G. Kevrekidis, P. Engels, V. Achilleos, D. J. Frantzeskakis, and J. Cuevas, J. Phys. B **45**, 115301 (2012).
- [18] W. H. Zurek, Phys. Rev. Lett. **102**, 105702 (2009); B. Damski and W. H. Zurek, Phys. Rev. Lett. **104**, 160404 (2010).
- [19] C. Weiler, T. Neely, D. Scherer, A. Bradley, M. Davis, and B. Anderson, Nature **455**, 948 (2008).
- [20] A. Vilenkin and E. P. S. Shellard, Cosmic Strings and Other Topological Defects (Cambridge University Press, Cambridge, 2000).
- [21] H. Takeuchi, S. Ishino, and M. Tsubota, Phys. Rev. Lett. **105**, 205301 (2010); S. Ishino, M. Tsubota, and H. Takeuchi, Phys. Rev. A **83**, 063602 (2011).
- [22] K. Fujimoto and M. Tsubota, Phys. Rev. A **85**, 033642 (2012).
- [23] D. Kobayakov, A. Bezett, E. Lundh, M. Marklund, and V. Bychkov, Phys. Rev. A **85**, 013630 (2012).
- [24] D. Kobayakov, V. Bychkov, E. Lundh, A. Bezett, and M. Marklund Phys. Rev. A **86**, 023614 (2012).
- [25] I. Danshita and L. Mathey, Phys. Rev. A **87**, 021603(R) (2013).
- [26] V. K. Mel'nikov, Lett. Math. Phys. **7**, 129 (1983); Phys. Lett. A **118**, 22 (1986); *ibid.* **128**, 9 (1988); *ibid.* **133**, 493 (1988).
- [27] V. Hakim, Phys. Rev. E **55**, 2835 (1997).
- [28] N. Pavloff, Phys. Rev. A **66**, 013610 (2002); A. Radouani, Phys. Rev. A **70**, 013602 (2004); G. Theocharis, P. G. Kevrekidis, H. E. Nistazakis, D. J. Frantzeskakis, A. R. Bishop, Phys. Lett. A, **337**, 441 (2005); R. Carretero-González, P. G. Kevrekidis, D. J. Frantzeskakis, B. A. Malomed, S. Nandi, A. R. Bishop, Math. Comput. Simul. **74**, 361 (2007); H. Susanto, P. G. Kevrekidis, R. Carretero-González, B. A. Malomed, D. J. Frantzeskakis, and A. R. Bishop, Phys. Rev. A **75**, 055601 (2007); Yu. G. Gladush, L. A. Smirnov, and A. M. Kamchatnov, J. Phys. B **41**, 165301 (2008); Yu. G. Gladush, A. M. Kamchatnov, Z. Shi, P. G. Kevrekidis, D. J. Frantzeskakis, and B. A. Malomed, Phys. Rev. A **79**, 033623 (2009); L. Y. Kravchenko and D. V. Fil, J. Low Temp. Phys. **155**, 219 (2009); A. S. Rodrigues, P. G. Kevrekidis, R. Carretero-González, D. J. Frantzeskakis, P. Schmelcher, T. J. Alexander, and Yu. S. Kivshar, Phys. Rev. A **79**, 043603 (2009).
- [29] T. W. Neely, E. C. Samson, A. S. Bradley, M. J. Davis, and B. P. Anderson, Phys. Rev. Lett. **104**, 160401 (2010).
- [30] K. M. Mertes, J. W. Merrill, R. Carretero-González, D. J. Frantzeskakis, P. G. Kevrekidis, and D. S. Hall, Phys. Rev. Lett. **99**, 190402 (2007).
- [31] V. P. Mineev, Zh. Eksp. Teor. Fiz. **67**, 263 (1974) [Sov. Phys. JETP **40**, 132 (1974)].
- [32] L. D. Carr, C. W. Clark, and W. P. Reinhardt, Phys. Rev. A **62**, 063610 (2000).
- [33] Y. Kawaguchi and M. Ueda, Phys. Rep **520**, 253 (2012).
- [34] K. J. H. Law, P. G. Kevrekidis, and L. S. Tuckerman, Phys. Rev. Lett. **105**, 160405 (2010).
- [35] M. Pola, J. Stockhofe, P. Schmelcher, and P. G. Kevrekidis Phys. Rev. A **86**, 053601 (2012).